JACS
JOURNAL OF THE AMERICAN CHEMICAL SOCIETY
Article
pubs.acs.org/JACS

Selective Photoreduction of Nitric Oxide to Nitrogen by Nanostructured TiO_2 Photocatalysts: Role of Oxygen Vacancies and Iron Dopant

Qingping Wu and Roel van de Krol*

Materials for Energy Conversion and Storage (MECS), Department of Chemical Engineering, Delft University of Technology, P.O. Box 5045, 2600 GA Delft, The Netherlands

ABSTRACT: Conventional TiO_2-based photocatalysts oxidize NO_x to nitrate species, which do not spontaneously desorb and therefore deactivate the catalyst. We show that the selectivity of this reaction can be changed by creating a large concentration of oxygen vacancies in TiO_2 nanoparticles through thermal reduction in a reducing atmosphere. This results in the photo*reduction* of nitric oxide (NO) to N_2 and O_2, species which spontaneously desorb at room temperature. The activity of the photoreduction reaction can be greatly enhanced by doping the TiO_2 nanoparticles with Fe^{3+}, an acceptor-type dopant that stabilizes the oxygen vacancies. Moreover, the photoinduced reduction of Fe^{3+} to Fe^{2+} provides a recombination pathway that almost completely suppresses the formation of NO_2 and thus enhances the selectivity of the reaction for N_2 formation. Gas chromatography confirms that N_2 and O_2 are formed in a stoichiometric ratio, and the activity for NO decomposition is found to be limited by the concentration of oxygen vacancies. A series of internally consistent reaction equations are proposed that describe all experimentally observed features of the photocatalytic process. The observed influence of oxygen vacancies on the activity and selectivity of photoinduced reactions may lead to new routes toward the design of highly selective photocatalysts.

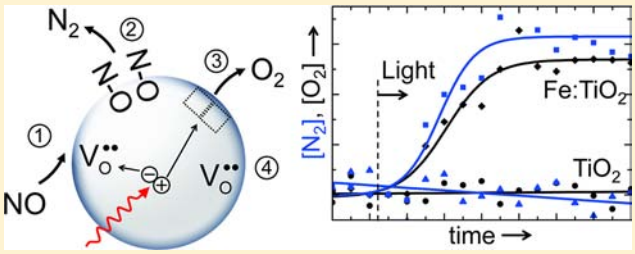

INTRODUCTION

Most of the world's energy consumption is based on the oxidation of fossil fuels in air. Examples are internal combustion engines in cars and turbines for power generation plants. These processes produce massive amounts of greenhouse gases, such as CO_2 and NO_x. NO_x (a mixture of NO and NO_2)[1] is formed when atmospheric nitrogen and oxygen react as a result of the high temperatures that are reached during fuel combustion.[2,3] Over the past few decades, atmospheric NO_x concentrations have greatly increased because of the growing number of automobiles and growing industrial activities.[4] This is reason for concern, since the emission of NO_x causes damage to human lung tissue and contributes to the formation of acid rain.[5] TiO_2, one of the best-known semiconductor photocatalysts, can decompose NO_x at room temperature and ambient pressure and has been widely studied for this purpose.[6−9] When TiO_2 is irradiated with photon energies exceeding its band gap of ~3.2 eV,[10] electrons are excited from the valence band (VB) to the conduction band (CB), resulting in the formation of electron−hole (e^-−h^+) pairs. A certain fraction of these charge carriers are able to reach the surface of the TiO_2 and are captured by surface-adsorbed species on Ti sites to form superoxide anions and hydroxyl radicals.[11,12] The free radicals are very active and can react with NO to form nitrates.[13] The main problem of this approach, however, is that these nitrates cannot spontaneously desorb. These species therefore deactivate the photocatalyst's surface, reducing the material's ability to remove NO_x from air. To avoid deactivation, the nitrates need to be washed away by rain.[14] The resulting nitric acid is corrosive and could pollute the soil when the concentration becomes too high. The removal of NO_x from air without deactivation and secondary pollution is therefore an urgent and demanding challenge.

One of the most promising ways to resolve this problem is to change the selectivity of the photocatalytic reaction so that NO_x is converted to N_2 and O_2. No deactivation would occur for this photoreduction reaction since nitrogen and oxygen readily desorb from the surface.[15] As reported by Anpo et al.,[16] the selectivity toward NO photoreduction can be greatly improved by reducing the coordination number of Ti^{4+} from its usual value of 6 (TiO_6 octahedra) to 4 (TiO_4 tetrahedra). This has been successfully achieved by depositing isolated TiO_4 clusters inside the cavities of zeolite-Y with ion beam implantation.[16,17] However, the large-scale application of zeolites with ion beam implantation techniques is economically unattractive.

In this paper, we propose a new strategy to change the photocatalytic selectivity of TiO_2 based on the creation of a large and stable concentration of oxygen vacancies. We will show that this indeed results in the photoreduction of NO to N_2 and O_2 and that the photo-oxidation reaction can be largely

Received: March 7, 2012
Published: May 18, 2012

suppressed. A series of reaction mechanisms that explain these observations will be given.

■ EXPERIMENTAL SECTION

Synthesis of Fe-doped TiO_2 thin films. A simple, template-free sol−gel method was employed for synthesizing pure TiO_2 and Fe-doped TiO_2 (Fe/TiO_2) colloidal solutions.[18] Briefly, titanium isopropoxide (TTIP; Acros, 98+%) was dropwise added to ultrapure water, slightly acidified with nitric acid, under vigorous stirring. For the preparation of Fe-doped TiO_2 samples, a certain amount of $Fe(NO_3)_3{\cdot}9H_2O$ was dissolved into the aqueous solution before addition of the TTIP. After hydrolysis of TTIP in the aqueous solution, an opaque suspension was obtained, which contains TiO_2 and propanol as the main reaction products. A homogeneous colloidal solution was produced after evaporation of the propanol at 333 K in a rotary evaporator. Fe-doped TiO_2 powders were synthesized with different Fe concentrations ranging from 0% Fe (undoped) to 1% Fe (atomic Fe/Ti ratio). Both TiO_2 and Fe/TiO_2 mesoporous films were fabricated by tape casting 300 μL sample solutions onto blank glass substrates (Schott Borofloat 33, 10 × 5 cm^2). The solutions were made by mixing 2 mL of the colloid (density 0.130 g/mL) with 180 μL of 10% Triton X-100 in H_2O and 0.02 g of polyethylene glycol. After tape casting, the films (area 10 × 3.8 cm^2) were dried in air to evaporate the water and fired at 723 K in air to remove any remaining organic components. The same method, but without the tape casting step, was used to convert part of the Fe/TiO_2 colloidal solutions into powders.

Structural Characterization. The crystal structures of Fe-doped TiO_2 and pure TiO_2 nanoparticles were analyzed by X-ray diffraction (XRD; Bruker D8 Advance) using Co Kα radiation (λ = 0.178897 nm). The specific surface areas of the powder samples were determined by Brunauer−Emmett−Teller (BET) adsorption measurements on a Quantachrome Autosorb-6B instrument at 77 K in liquid nitrogen. Prior to these measurements, the samples were pretreated in vacuum at 623 K for 16 h. The Raman spectra were recorded by a Renishaw Raman imaging microscope (system 2000). A 514.5 nm Ar^+ laser line with a power output of 20 mW was used for excitation. A Leica DMLM optical microscope with a Leica PL floutar L500/5 objective lens was used to focus the beam on the sample. The 520 cm^{-1} peak of a Si wafer served as a wavelength reference for the Raman spectra.

Activity Measurements. The photocatalytic activity of the samples was evaluated in a continuous-flow setup (Figure 1) equipped with an online chemiluminescence-based NO_x analyzer (Teledyne Instruments, model 200E) with a measurement range of 0−2 ppm. The samples were placed in a 10 cm wide reactor trough, 5 mm below a fused silica optical window, consistent with international standard NEN-ISO 22197-1:2007. A continuous 1 L/min flow of ∼1000 ppb NO in air, pure N_2, or pure He (Linde Gas Belgium NV) passed over the sample surface, which was irradiated by a UV light source (75 W facial tanner, Philips HB172) with an intensity of ∼2 mW/cm^2. The NO and NO_x (= NO + NO_2) concentrations were continuously recorded every 10 s, while the NO_2 concentration was automatically calculated by the analyzer from the concentration difference between NO_x and NO.

The N_2 and O_2 concentrations were measured by online gas chromatography. The gas chromatograph (Shimadzu, GC-2014) was equipped with a pulsed discharge detector (PDD) operating at 493 K. The photocatalytic products were separated by a combination of Porapak Q and GsBP-PLOT molsieve columns using pure helium (99.9999%) as the carrier gas. To exceed the detection limit of the gas chromatograph, a flow of 100 ppm NO in He was used as the target pollutant for GC measurements.

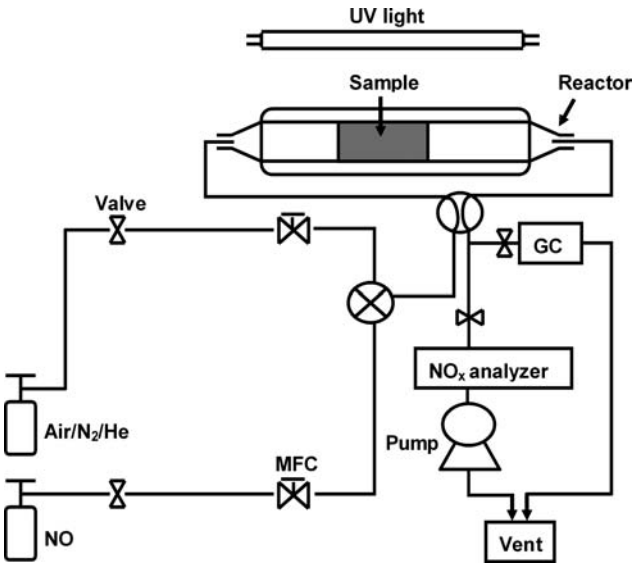

Figure 1. Schematic diagram of the continuous-flow NO_x photocatalytic setup. Air, pure nitrogen, or helium was used as the carrier gas.

■ RESULTS AND DISCUSSION

To investigate the influence of oxygen vacancies on the decomposition of NO over undoped TiO_2, the photocatalytic activity for stoichiometric TiO_2 (as-prepared TiO_2 that is fully oxidized by a heat treatment at 723 K in air) and reduced TiO_2 (heat treatment at 723 K in a 2% H_2/Ar atmosphere) are compared. The results are shown in Figure 2, and we briefly describe the overall features here before presenting more detailed reaction schemes later in this paper. The photocatalytic reactions are initiated by illuminating the sample with UV light after 1 h of equilibration in a ∼1 ppm NO atmosphere in the dark. For oxidized TiO_2, the NO concentration immediately decreases by ∼800 ppb upon illumination (Figure 2a). This is due to the reaction of gas-phase NO species with adsorbed superoxide anions (O_2^-), resulting in the formation of nitrate groups. The superoxide anions are formed by the reduction of adsorbed O_2 by photoexcited electrons. Since the nitrate groups do not spontaneously desorb, the surface slowly saturates and the NO concentration at the reactor outlet increases again.[14,19]

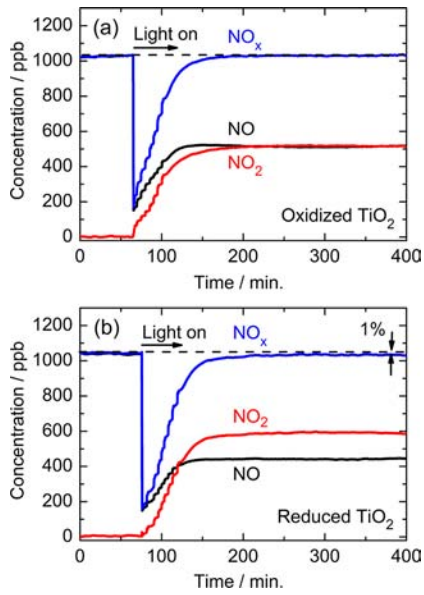

Figure 2. Photocatalytic degradation of NO in air for (a) oxidized and (b) reduced TiO_2 under UV light irradiation.

Integration of the NO_x peak area below the 1040 ppb baseline in Figure 2a yields a total number of 0.69×10^{18} nitrate adsorbates, which corresponds to ~5% of the total number of surface sites (~1.3×10^{19} cm^{-2}, based on 0.019 g of TiO_2, a BET surface area of 71 m^2/g, and a surface site density of 1×10^{15} cm^{-2} for 5-fold-coordinated Ti^{4+} at the lowest energy {101} surface[20]). At the same time, 50% of the NO is photo-oxidized to NO_2 at the illuminated TiO_2 surface via reaction of NO with photogenerated hydroxyl radicals. This undesired reaction (the toxicity of NO_2 exceeds that of NO) also occurs in air, but under ambient conditions the process is very slow. Clearly, illuminated TiO_2 strongly catalyzes this reaction. After ~200 min, the surface is fully saturated with nitrate groups and no net change in the NO_x concentration occurs anymore.

Reduced TiO_2 shows a slightly higher activity for the photo-oxidation of NO to NO_2 than oxidized TiO_2 under otherwise identical conditions (Figure 2b). We attribute this to the presence of oxygen vacancies that are formed during the reduction treatment.[21] Using standard Kröger–Vink notation,[22] the corresponding reaction can be written as

$$O_O^{\times} \overset{TiO_2}{\rightleftharpoons} V_O^{\bullet\bullet} + 2e' + \tfrac{1}{2}O_2(g) \quad (1)$$

In-plane vacancies such as these, or step or kink sites, are well-known to be able to enhance the catalytic activity for certain reactions by providing energetically favorable ad- or desorption sites.[23−26]

A less pronounced but arguably more important observation from the data in Figure 2b is that, after the surface is saturated with NO_3^- groups, the sum of the NO and NO_2 concentrations is no longer equal to the initial NO concentration of 1040 ppb. About 1% of the NO_x (10 ppb) has disappeared and must have been converted to another species. Since NO_3^- and NO_2 are the only stable oxidation products after NO conversion, we attribute the 1% "lost" NO_x to the formation of a reduction product, such as N_2O or N_2.

Although the 1% lost NO_x can be accurately and very reproducibly measured, the amount is rather small. We attribute this to the fact that reaction 1 is reversible, which causes part of the reduced TiO_2 to be reoxidized while exposed to air. Before exploring further evidence for the photoreduction reaction and possible mechanisms that cause it, we first need to stabilize the oxygen vacancies in reduced TiO_2. This can be achieved by doping the TiO_2 nanoparticles with Fe, a process that we recently studied in detail.[27] The Fe^{3+} substitutes for Ti^{4+} ions in the lattice, and the effective negative charge of this acceptor-type dopant is compensated by the positively charged oxygen vacancies. The reaction for the dissolution of iron in TiO_2 can be written as follows:

$$Fe_2O_3 \xrightarrow{TiO_2, 773\,K} 2Fe_{Ti}' + V_O^{\bullet\bullet} + 3O_O^{\times} \quad (2)$$

Evidence for the formation of oxygen vacancies upon Fe doping is provided by a combination of X-ray diffraction (XRD) and Raman measurements (Figure 3). The XRD patterns show that the d_{101} lattice spacing decreases linearly with increasing Fe concentration (Figure 3a), which proves that Fe ions are indeed incorporated as dopants in the TiO_2 lattice. The fact that the lattice spacing decreases, even though Fe^{3+} is slightly larger than Ti^{4+},[28] is due to the formation of oxygen vacancies.[27] Further evidence for the presence of oxygen vacancies is given by Raman spectroscopy. As indicated in Figure 3b, the Raman peak position of the anatase E_g mode shows a linear shift with increasing Fe concentration. Such a shift was first observed for reduced (undoped) anatase TiO_2 by Parker et al.,[29,30] who were able to relate the size of the shift to the oxygen stoichiometry. Parker's results are plotted in Figure 3b (dashed line) on the same x-axis scale, using the assumption that one oxygen vacancy is formed for every two Fe ions (see eq 2). The slopes of the data points and the dashed line are identical. Together with the XRD data, this confirms that the Fe dopants are indeed fully charge-compensated by oxygen vacancies.[27]

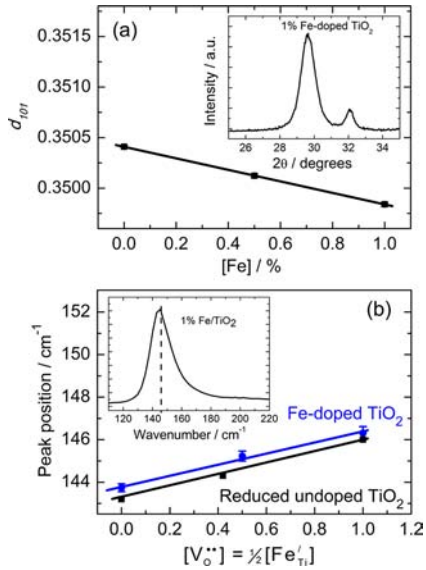

Figure 3. (a) Shift of the anatase (101) peak as a function of the Fe concentration in Fe/TiO_2 nanoparticles. The XRD pattern in the inset shows that anatase (main peak) is the dominant phase, with only a small amount of rutile (peak at 32°). (b) Position of the anatase E_g Raman peak (inset) as a function of the Fe concentration for Fe/TiO_2 (this study) and as a function of the oxygen stoichiometry for undoped TiO_2 (Parker et al.[29]).

The degradation of NO over Fe-doped TiO_2 is shown in Figure 4a. The initial stage of the reaction after the light is turned on is similar to that observed for undoped TiO_2: a fast

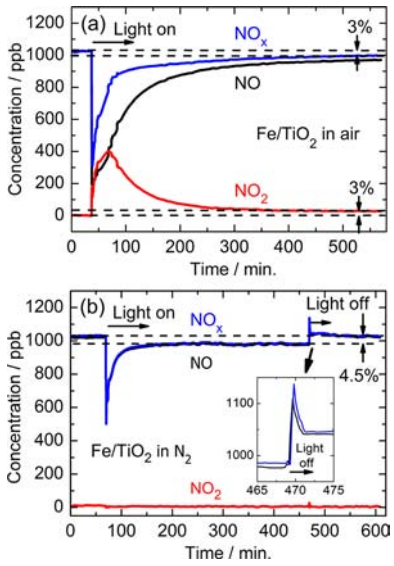

Figure 4. Photocatalytic degradation of NO over 1% Fe/TiO_2 (a) in air and (b) in pure N_2.

decrease of the NO concentration (adsorption at photogenerated superoxide sites) followed by a slower increase of the NO signal as the surface becomes saturated with NO_3^- groups (deactivation). However, the amount of NO_x that is presumably "lost" to photoreduction has now increased to 3%. This is an increase of a factor of 3 compared to that of undoped reduced TiO_2. We attribute this large increase to the higher concentration of oxygen vacancies, which are now stabilized by the presence of charge-compensating Fe acceptors.

A second important observation in Figure 4a is that the formation of NO_2 is almost completely suppressed after 300 min. After steady-state conditions are reached, only 3% of the NO is continuously converted to NO_2. This is much less than the 50−60% observed for undoped TiO_2 (Figure 2). Apparently, Fe doping strongly suppresses the *activity* for NO_2 formation, but also increases the *selectivity* toward photoreduction from 0% to 50% (3% reduction + 3% oxidation).

To further prove the ability of 1% Fe-doped TiO_2 to photoreduce NO, pure N_2 (99.999%) was used instead of air as the carrier gas for the NO pollutant. Figure 4b shows that, even in the absence of oxygen, 4.5% of the NO_x continuously disappears after reaching steady-state conditions. This is again consistent with what would be expected for an overall photoreduction reaction.

It should be noted that, even in a N_2 atmosphere, the NO concentration briefly decreases during the first 50 s after the light is turned on (Figure 4b). As outlined above, this is due to the reaction of NO with adsorbed O_2^- species, resulting in the formation of NO_3^-. The O_2^- species are formed while the sample is exposed to air and ambient light prior to the experiment and do not spontaneously desorb after replacement of the air in the reactor chamber with N_2. Further inspection of Figure 4b shows that no NO_2 is formed during the initial and steady-state phases of the photoreaction. This indicates that the selectivity for photoreduction is 100% for 1% Fe-doped TiO_2 in the absence of oxygen.

A final observation from Figure 4b is the immediate desorption of a small amount of NO after the UV light is turned off. This indicates the presence of a small amount of unreacted, adsorbed NO at the TiO_2 surface. From integration of the desorption peak, the amount of desorbed NO corresponds to ∼0.04% of the total number of TiO_2 surface sites.[31] This is a much smaller fraction than the number of adsorbed nitrate species mentioned before, which suggests that NO quickly reacts to NO_3^- after being adsorbed.

To support our assumption that the lost NO in Figure 4 is photocatalytically reduced, gas chromatography measurements were carried out to identify the chemical nature of the reaction product(s). This indeed revealed the presence of N_2 and O_2, while no other species (such as N_2O) were detected. The absence of N_2O can be explained by the absence of lateral interactions between adsorbed NO species at these low NO concentrations.[32] As shown in Figure 5, the concentrations of N_2 and O_2 gradually increase until steady-state conditions are reached after ∼80 min. Both gases evolve in a stoichiometric ratio, which is consistent with the absence of N_2O formation. It should be noted that the sum of the N_2 and O_2 concentrations is ∼1% of the initial NO concentration, i.e., 4.5 times less than the fraction of NO converted in Figure 4b. We attribute this to the 100-fold larger total concentration of NO used for the GC experiment. Such a large concentration may saturate the total number of available reaction sites at the surface, explaining the

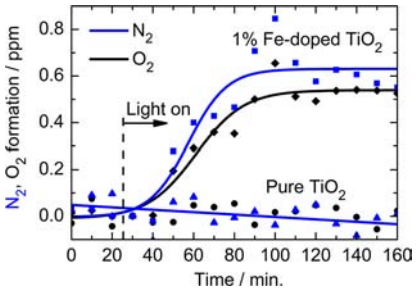

Figure 5. Photocatalytic conversion of NO to N_2 and O_2 over 1% Fe-doped TiO_2. The sample was irradiated with UV light, and the target pollutant was 100 ppm NO in He.

lower fractional conversion. A control experiment with undoped TiO_2, also shown in Figure 5, did not show any N_2 or O_2 evolution. This clearly shows that Fe doping of TiO_2 changes its photocatalytic selectivity for NO degradation from oxidation to reduction.

On the basis of all these observations, we propose the following series of reactions to describe the various processes that occur.

Photo-Oxidation of NO to NO_2 and NO_3^-. The reaction of photoinduced electrons and holes with surface-adsorbed oxygen and hydroxyl groups results in the formation of superoxide anions and hydroxyl radicals:[11,12]

$$h\nu \xrightarrow{TiO_2} e^- + h^+ \tag{3}$$

$$Ti(O_2)_{ads} + e^- \xrightarrow{k_1} Ti(O_2^-)_{ads} \tag{4}$$

$$Ti{-}OH^- + h^+ \rightarrow Ti{-}OH^\bullet \tag{5}$$

The superoxide anion can directly oxidize nitric oxide to a nitrate adsorbate:

$$Ti(O_2^-)_{ads} + NO(g) \rightarrow Ti(NO_3^-)_{ads} \tag{6}$$

At the same time, photo-oxidation of NO by hydroxyl radicals leads to the formation of NO_2:

$$Ti{-}OH^\bullet + NO \rightarrow Ti{-}H + NO_2(g) \tag{7}$$

While the Ti−H bond seems unusual, density functional theory (DFT) calculations suggest that it can indeed exist at the (001), (100), and (101) surfaces of anatase (the hydrogen binds to undercoordinated Ti atoms, resulting in a Ti−H bond length of ∼1.75 Å and a slightly outward relaxation of the Ti atoms).[33] At the initial stage of the reaction (before the steady state is reached), the net overall reaction can thus be summarized as

$$Ti(O_2)_{ads} + Ti{-}OH^- + h\nu + 2NO(g) \rightarrow Ti(NO_3^-)_{ads} + Ti{-}H + NO_2(g) \tag{8}$$

The sum reaction 8 indicates that NO_2 and NO_3^- are simultaneously produced, consistent with the data shown in Figure 2a.

Since the adsorbed nitrate groups do not spontaneously desorb, reactions 4 and 6 will stop after a while and the catalyst slowly deactivates. Since NO_2 formation via photogenerated holes—reactions 5 and 7—persists after deactivation, there must be an alternative reaction path for the photogenerated electrons under steady-state conditions. A likely pathway is the following:[12,34]

$$\text{Ti–H} + O_2(g) + e^- \xrightarrow{k_2} \text{Ti–OOH}^- \quad (9)$$

$$\text{Ti–OOH}^- + \text{Ti–H} \rightarrow \text{Ti–OH}^- + \text{Ti–OH}^\bullet \quad (10)$$

$$\text{Ti–OH}^\bullet + e^- \rightarrow \text{Ti–OH}^- \quad (11)$$

Under steady-state conditions, reactions 3, 5, 7, and 9–11 all occur simultaneously and can be summed up to give

$$2NO(g) + O_2(g) + 2h\nu \xrightarrow{TiO_2} 2NO_2(g) \quad (12)$$

Suppression of NO_2 Formation. The presence of Fe^{3+} markedly changes the reaction mechanism for NO_2 formation, as illustrated by Figure 4a. During the initial stage of illumination, NO_2 is again formed via the mechanism described by reaction 8. However, instead of regenerating Ti–H sites via reactions 9–11 after deactivation, the photogenerated electrons can now reduce Fe^{3+}:

$$Fe^{3+} + e^- \xrightarrow{k_3} Fe^{2+} \quad (13)$$

Fe^{2+} is a well-known adsorption site for nitric oxide, leading to the formation of mono- or dinitrosyl species:[35,36]

$$Fe^{2+} + nNO(g) \rightarrow Fe^{2+}(NO)_{n,ads} \quad (14)$$

where n equals 1 or 2, respectively. This species can be oxidized again via adjacent hydroxyl radicals or by direct capture of photogenerated holes:

$$Fe^{2+}(NO)_{n,ads} + \text{Ti–OH}^\bullet \rightarrow Fe^{3+}(NO)_{n,ads} + \text{Ti–OH}^- \quad (15a)$$

$$Fe^{2+}(NO)_{n,ads} + h^+ \rightarrow Fe^{3+}(NO)_{n,ads} \quad (15b)$$

The oxidation of Fe^{2+} to Fe^{3+} reduces the degree of π back-bonding, which weakens the Fe^{3+}–NO bond and results in desorption:[18]

$$Fe^{3+}(NO)_{n,ads} \rightarrow Fe^{3+} + nNO(g) \quad (16)$$

The sum of reactions 3, 5, 13, 14, 15a, and 16 represents a NO-mediated recombination mechanism that explains why so little NO_2 is formed over Fe-doped TiO_2 after steady-state conditions are reached.

The formation of $Fe^{2+}(NO)_n$ species via reaction 14 is supported by the immediate release of NO to the gas phase (reaction 16) when the UV light is turned off, as shown in Figure 4b. Note that this observation also rules out reaction 15b, since no holes are available in the dark. Reaction 15a therefore seems a more likely pathway for reoxidation of Fe^{2+}.

Photoreduction. The formation of N_2 and O_2 (Figure 5) can occur via at least two different routes. One possibility is that a small amount of tetrahedrally coordinated Ti is formed in the Fe-doped TiO_2 samples. This species has been reported as the active site for catalytic decomposition of NO into N_2 and O_2 at Ti-modified zeolites by Anpo and co-workers.[17,37] Since most Ti ions at the TiO_2 surface are 5-fold-coordinated, a single oxygen vacancy created at or near the surface could indeed lead to a 4-fold-coordinated Ti^{4+} center. However, the Ti–O bond length would still be similar to the 1.93 Å found in bulk TiO_2, whereas the tetrahedrally coordinated TiO_4 centers that are reported to photoreduce NO to N_2 have a significantly smaller bond length (~1.78 Å).[38] Such a strong reduction in bond length would require very high oxygen vacancy concentrations, much higher than those present in our 1% Fe-doped TiO_2.[27] On the basis of these arguments, the possibility that the formation of N_2 and O_2 is due to tetrahedrally coordinated Ti^{4+} seems unlikely.

A more plausible explanation is that oxygen vacancies act as catalytic centers that capture the oxygen end of the NO molecules:

$$V^{\bullet\bullet}_{O(surf)} + 2e^- + NO(g) \rightarrow O_{surf}\text{–N} \quad (17)$$

Since the captured NO molecules have no net charge, mobile oxygen vacancies[39] are able to diffuse close to the captured molecule and capture another NO molecule on a neighboring site. Alternatively, the O_{surf}–N species themselves may be sufficiently mobile—for example, via a surface vacancy diffusion mechanism—to meet each other. They can then react to form N_2:

$$2O_{surf}\text{–N} \rightarrow 2O_{surf} + N_2(g) \quad (18)$$

Since N_2 has a higher thermodynamic stability than NO ($\Delta G^0_f(NO)$ = +87.6 kJ/mol), reaction 18 will be exothermic. The released energy helps to release the trapped oxygen atoms from the lattice sites, resulting in the formation of O_2:

$$2O_{surf} \rightarrow 2V^{\times}_O + O_2(g) \quad (19)$$

The photogenerated holes (h^+) can then reoxidize the neutral oxygen vacancies to their normal 2+ state:

$$V^{\times}_O + 2h^+ \rightarrow V^{\bullet\bullet}_O \quad (20)$$

Summing up reactions 3 and 17–20 gives the overall photoreduction reaction

$$2NO(g) + 4h\nu \xrightarrow{2V^{\bullet\bullet}_O} N_2(g) + O_2(g) \quad (21)$$

Repeating the experiment of Figure 4b for a longer time showed no change in the fraction of NO that is lost to photoreduction; a value of 4.5% was found even after 1050 min. This corresponds to a turnover number of ~2 nitric oxide molecules per oxygen vacancy site, which confirms that this defect acts as a catalytic center.

Before any further attempts can be made to improve the photocatalytic activity of the material, it is important to identify the rate-limiting factor of the overall photoreduction process. Possible external factors include the illumination intensity and the concentration of oxygen vacancies. The influence of the UV light intensity on NO decomposition for 1% Fe-doped TiO_2 is shown in Figure 6. Clearly, the photon flux is not a limiting factor in this range of light intensities.

The influence of oxygen vacancies on the photocatalytic activity is investigated by repeating the experiment of Figure 4b with half the concentration of oxygen vacancies (0.5% instead of 1% Fe; all other conditions are the same). As shown in

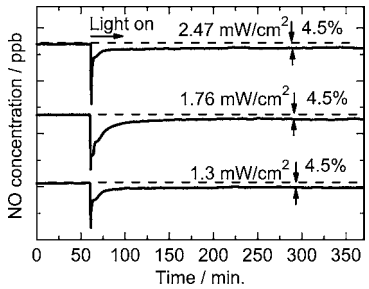

Figure 6. Influence of the UV light intensity on the photocatalytic activity for NO degradation of 1% Fe-doped TiO_2 in pure N_2.

dx.doi.org/10.1021/ja302246b | J. Am. Chem. Soc. 2012, 134, 9369–9375

Figure 7, the NO conversion efficiency is 3%, significantly less than the 4.5% in Figure 4b. This shows that the concentration of oxygen vacancies indeed limits the photocatalytic activity for NO reduction. Further improvements of this system may therefore be possible by increasing the concentration of Fe. We recently showed that Fe dopant concentrations of up to 10% in TiO_2 nanoparticles are possible before segregation of iron oxide occurs.[27]

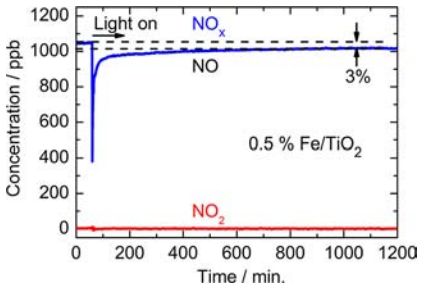

Figure 7. Photocatalytic decomposition of NO for 0.5% Fe/TiO_2 in pure N_2.

CONCLUSIONS

We have found that oxygen vacancies in nanosized TiO_2 serve as active centers for the photocatalytic reduction of nitric oxide into N_2 and O_2. By doping the material with Fe, the mechanism of the reaction can be influenced in two distinct ways: (i) Fe^{3+} is an acceptor-type dopant that stabilizes the oxygen vacancies through charge compensation, thereby increasing the *activity* of the photoreduction reaction, and (ii) Fe^{3+} can be photoreduced to Fe^{2+}, providing a recombination pathway that suppresses the formation of NO_2 and thus enhances the *selectivity* of the reaction for N_2 formation. While the conversion efficiency is still modest, the Fe/TiO_2 photocatalyst does not show any signs of deactivation. In contrast to the standard $DeNO_x$ catalysts based on TiO_2, the conversion is not blocked by nitrate species that have to be washed away periodically. The material is also easier and cheaper to synthesize than NO photoreduction catalysts based on modified zeolites.

Further improvement of the photocatalytic activity seems simply a matter of increasing the dopant concentration. For Fe, dopant concentrations of up to 10% have been reported, which leaves ample room for further optimization. Alternatively, other acceptor-type dopants can be explored. On the basis of the proposed reaction mechanisms, it is important to choose dopants that can be reduced to the 2+ oxidation state to avoid the oxidation of NO to NO_2. Cr, Co, and Ni are therefore more suitable choices than, e.g., Al or Ga. Further explorations along these lines may lead to a new generation of highly selective photocatalysts.

AUTHOR INFORMATION

Corresponding Author
r.vandekrol@tudelft.nl

Notes
The authors declare no competing financial interest.

ACKNOWLEDGMENTS

We gratefully acknowledge Prof. D. Bahnemann (Leibniz Universität Hannover, Germany) for advice and J. Middelkoop for practical help with setting up the NO_x analysis system. We thank B. Boshuizen for designing a Labview program to read the NO_x analyzer. Financial support for this work is provided by the Shell-TU Delft "Sustainable Mobility" program.

REFERENCES

(1) Devahasdin, S.; Fan, C.; Li, K.; Chen, D. H. *J. Photochem. Photobiol., A* **2003**, *156*, 161−170.
(2) Roy, S.; Baiker, A. *Chem. Rev.* **2009**, *109*, 4054−4091.
(3) Wu, J. C. S.; Cheng, Y. *J. Catal.* **2006**, *237*, 393−404.
(4) Taylor, K. C. *Catal. Rev.—Sci. Eng.* **1993**, *35*, 457−481.
(5) Rodriguez, J. A.; Jirsak, T.; Liu, G.; Hrbek, J.; Dvorak, J.; Maiti, A. *J. Am. Chem. Soc.* **2001**, *123*, 9597−9605.
(6) Maggos, T.; Bartzis, J. G.; Liakou, M.; Gobin, C. *J. Hazard. Mater.* **2007**, *146*, 668−673.
(7) Negishi, N.; Takeuchi, K.; Ibusuki, T. *J. Mater. Sci.* **1998**, *33*, 5789−5794.
(8) Lin, Y. M.; Tseng, Y. H.; Huang, J. H.; Chao, C. C.; Chen., C. C.; Wang, I. *Environ. Sci. Technol.* **2006**, *40*, 1616−1621.
(9) Anpo, M. *Pure Appl. Chem.* **2000**, *72*, 1265−1270.
(10) Wang, J.; Tafen, D. N.; Lewis, J. P.; Hong, Z.; Manivannan, A.; Zhi, M.; Li, M.; Wu, N. *J. Am. Chem. Soc.* **2009**, *131*, 12290−12297.
(11) Du, Y.; Rabani, J. *J. Phys. Chem. B* **2003**, *107*, 11970−11978.
(12) Hoffmann, M. R.; Martin, S. T.; Choi, W.; Bahnemann, D. W. *Chem. Rev.* **1995**, *95*, 69−96.
(13) Dalton, J. S.; Janes, P. A.; Jones, N. G.; Nicholson, J. A.; Hallam, K. R.; Allen, G. C. *Environ. Pollut.* **2002**, *120*, 415−422.
(14) Wang, H.; Wu, Z.; Zhao, W.; Guan, B. *Chemosphere* **2007**, *66*, 185−190.
(15) Anpo, M.; Zhang, S. G.; Mishima, H.; Matsuoka, M.; Yamashita, H. *Catal. Today* **1997**, *39*, 159−168.
(16) Anpo, M.; Takeuchi, M.; Ikeue, K.; Dohshi, S. *Curr. Opin. Solid State Mater. Sci.* **2002**, *6*, 381−388.
(17) Yamashita, H.; Ichihashi, Y.; Zhang, S. G.; Matsumura, Y.; Souma, Y.; Tatsumi, T.; Anpo, M. *Appl. Surf. Sci.* **1997**, *121*, 305−309.
(18) Wu, Q.; Mul, G.; Van de Krol, R. *Energy Environ. Sci.* **2011**, *4*, 2140−2144.
(19) Komazaki, Y.; Shimizu, H.; Tananka, S. *Atmos. Environ.* **1999**, *33*, 4363−4371.
(20) Henningsson, A.; Andersson, M. P.; Uvdal, P.; Siegbahn, H.; Sandell, A. *Chem. Phys. Lett.* **2002**, *360*, 85−90.
(21) Liu, H.; Ma, H. T.; Li, X. Z.; Li, W. Z.; Wu, M.; Bao, X. H. *Chemosphere* **2003**, *50*, 39−46.
(22) Chiang, Y. M.; Birnie, D. P.; Kingery, W. D. *Physical Ceramics*; Wiley: New York, 1997.
(23) Gong, X. Q.; Selloni, A.; Batzill, M.; Diebold, U. *Nat. Mater.* **2006**, *5*, 665−670.
(24) Beck, T. J.; Klust, A.; Batzill, M.; Diebold, U.; Valentin, C. D.; Selloni, A. *Phys. Rev. Lett.* **2004**, *93*, 0361041−0361044.
(25) Thompson, T. L.; Yates, J. T. *Chem. Rev.* **2006**, *106*, 4428−4453.
(26) Henderson, M. A.; Epling, W. S.; Perkins, C. L.; Peden, C. H. F. *J. Phys. Chem. B* **1999**, *103*, 5328−5337.
(27) Wu, Q.; Zheng, Q.; Van de Krol, R. *J. Phys. Chem. C* **2012**, *116*, 7219−7226.
(28) Shannon, R. D. *Acta Crystallogr., A* **1976**, *32*, 751−767.
(29) Parker, J. C.; Siegel, R. W. *Appl. Phys. Lett.* **1990**, *57*, 943−945.
(30) Parker, J. C.; Siegel, R. W. *J. Mater. Res.* **1990**, *5*, 1246−1252.
(31) The number of desorbed NO molecules was determined by integrating the NO_x curve from t = 469 min to t = 471.5 min in Figure 4b. The final concentration of 1040 ppb was used as a baseline. This corresponds to 5.2×10^{15} NO molecules. On the basis of the mass of the sample (0.019 g) and a BET surface area of 71 m^2/g, this corresponds to ∼0.04% of the total amount of the sample's surface sites.
(32) Diebold, U. *Surf. Sci. Rep.* **2003**, *48*, 53−229.
(33) Barnard, A. S.; Zapol, P. *Phys. Rev. B* **2004**, *70*, 235403.
(34) Zhang, Z.; Wang, C.; Zakaria, R.; Ying, J. Y. *J. Phys. Chem. B* **1998**, *102*, 10871−10878.

(35) Mul, G.; Pérez-Ramírez, J.; Kapteijn, F.; Moulijn, J. A. *Catal. Lett.* **2002**, *3*, 129−138.
(36) King, D. L.; Peri, J. B. *J. Catal.* **1983**, *79*, 164−175.
(37) Hu, Y.; Martra, G.; Zhang, J.; Higashimoto, S.; Coluccia, S.; Anpo, M. *J. Phys. Chem. B* **2006**, *110*, 1680−1685.
(38) Yamashita, H.; Ichihashi, Y.; Anpo, M.; Hashimoto, M.; Louis, C.; Che, M. *J. Phys. Chem.* **1996**, *100*, 16041−16044.
(39) Schaub, R.; Wahlströn, E.; Rønnau, A.; Lægsgaard, E.; Stensgaard, I.; Besenbacher, F. *Science* **2003**, *299*, 377−379.